ACS APPLIED MATERIALS & INTERFACES

Research Article

www.acsami.org

Electrospun Cellulose Acetate-Garnet Nanocomposite Magnetic Fibers for Bioseparations

Imalka Munaweera, Ali Aliev, and Kenneth J. Balkus, Jr.*

Department of Chemistry and the Alan G. MacDiarmid Nanotech Institute, University of Texas at Dallas, 800 West Campbell Road, Richardson, Texas 75080, United States

Supporting Information

ABSTRACT: Cellulose acetate fibers with magnetic properties have recently attracted much attention because of their potential novel applications in biomedicine such as for cell and protein separations, magnetic resonance imaging contrast agents, and magnetic filters. In this work, as synthesized yttrium iron garnet and gadolinium substituted yttrium iron garnet nanoparticles have been used to generate magnetic filter paper. Garnet nanoparticles dispersed in cellulose acetate polymer solutions were electrospun as free-standing nonwoven fiber mats as well as on cellulose filter paper substrates resulting in magnetic filter papers. The magnetic fibers were characterized by scanning electron microscopy (SEM), transmission electron microscopy (TEM), powder X-ray diffraction (PXRD), and superconducting quantum interference device (SQUID) magnetic property measurements. The resulting magnetic polymer nanocomposites can be easily picked up by an external magnet from a liquid medium. Fluorescein isothiocyanate (FITC) labeled bovine serum albumin (BSA) was separated from solution by using the magnetic filter paper.

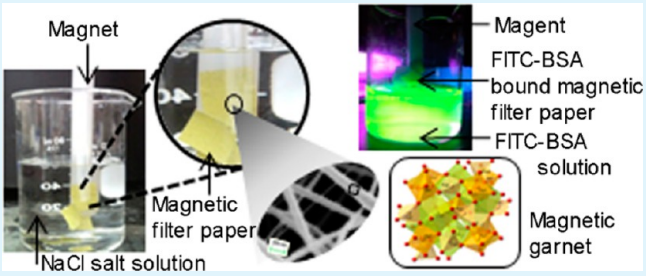

KEYWORDS: *magnetic, electrospinning, fibers, filter paper, bioseparations*

INTRODUCTION

Composite nanofibers consisting of magnetic nanoparticles embedded into a polymer matrix have been investigated because of their magnetic-field dependent physical properties. A large number of applications like magnetic cell and protein separation,[1,2] magnetic resonance imaging contrast agents,[3] magnetic filters,[4] magnetic sensors[5] and low frequency magnetic shielding[6] have been reported. In the area of biological and clinical applications, magnetic separation is an emerging technology that uses magnetism for the efficient separation of magnetic carriers from chemical or biological suspensions. A distinct advantage of magnetic separation is that there is less mechanical stress on the sample than in other methods such as column based techniques, precipitation, and centrifugation.[7]

In this research, electrospun cellulose acetate garnet nanocomposite magnetic fibers have been reported for the first time. The preparation of the biocompatible magnetic filter paper involves a cost-effective electrospining technique. A distinct advantage of the electrospun magnetic nanocomposite fibers compared with conventional bioseparation methods is that they can be used directly to separate crude samples containing suspended solid materials such as fermentation or culture medium and some biomolecules from aqueous systems without pretreatment in the presence of magnetic gradient fields. Magnetic hybrid hydrogels have been reported for magnetically assisted bioseparations. The hydrogels were fabricated by in situ embedding of magnetic iron oxide nanoparticles into the porous hydrogel network.[8] Magnetic Fe_2O_3/Au core/shell nanoparticles,[9] magnetic silica nanotubes,[10] magnetite containing spherical silica nanoparticles,[11] and magnetic nanoparticles with alkoxysilianes[12] have also been reported for bioseparations. The advantage of the magnetic electrospun filter paper is that it can be easily chemically functionalized for particular bioseparations because of the rich surface chemistry of cellulose acetate nanofibers, and the filter paper can be easily transferred in biological suspensions. Also these magnetic filter papers are easy to handle, flexible, inexpensive, and highly scalable. Most of the reported magnetic fibers are black in color[13] whereas these garnet based fibers are pale yellow in color which can easily be distinguished in biological suspensions.

Garnet nanoparticles have been used as magnetic additives where the magnetic properties mainly depend on composition, crystal structure, and temperature. Yttrium iron garnet (YIG) and yttrium gadolinium iron garnet (YGIG) are members of the isostructural garnet family.

The general formula for a garnet is $C_3A_2D_3O_{12}$ where the C cations occupy dodecahedral sites, the A cations occupy octahedral sites, and the D cations occupy tetrahedral sites in the crystal structure as shown in Figure 1. The oxygen atoms are indicated by red color. In the case of YIG, Y^{3+} occupies

Received: September 19, 2013
Accepted: December 16, 2013
Published: December 16, 2013

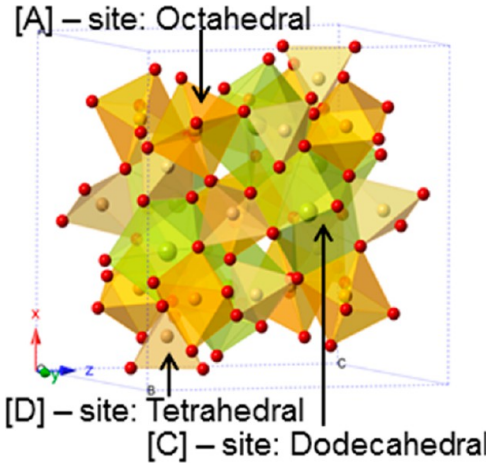

Figure 1. Crystal structure (cubic, *Ia3d*) of garnet calculated using the crystallographic data in reference14.

dodecahedral sites and Fe^{3+} occupies both octahedral and tetrahedral sites in the structure. A wide variety of cations in different valence states can reside in the cation sites where the primary consideration for site occupancy is ionic size. Thus many compositions form garnet structures that exhibit different magnetic properties.[15] Many rare earth iron garnets will form solid solution phases because of the similarity in ionic radii of the rare earth ions. In the case of yttrium(III) (ionic radius = 0.104 nm) and gadolinium(III) (ionic radius = 0.108 nm), the complete family of solid solutions can be prepared: $Y_xGd_{3-x}Fe_5O_{12}$ ($0 \leq x \leq 3$). Substitution of yttrium for gadolinium occurs at the dodecahedral sites since Gd^{3+} is slightly larger than Y^{3+}, an increase in the unit cell would be expected with increasing gadolinium content. The effect of crystallite size and magnetic properties of $Y_xGd_{3-x}Fe_5O_{12}$ have also been reported.[16] Various techniques have been used to prepare crystalline YIG nanopowders including coprecipitation,[17,18] sol–gel,[19,20] microemulsion,[21] organic precursor method,[22] hydrothermal[23] and mechanochemical[24] techniques. The chemical coprecipitation method is particularly attractive because of the low-cost and suitability for mass production.[25] Moreover, coprecipitation processing provides better mixing of the starting materials and excellent chemical homogeneity of the final product.

The polymeric nanofibers containing magnetic nanoparticles combine the properties of a polymeric nanofiber material, that is, high surface/volume ratio, good mechanical flexibility, surface functionality, and superior mechanical performance with magnetic properties.[26] A number of processing techniques including melt fibrillation,[27] nanolithography,[28] template synthesis,[29,30] self-assembly,[31] interfacial polymerization,[32] and electrospining[33−36] have been used to prepare polymeric nanofibers in recent years. Among these techniques, electrospinning has proven to be a versatile and effective method to prepare polymer fibers with diameters ranging from a few nanometers to micrometers or more.[37−39] Electrospinning is a technique which uses electrical charge to draw a polymer solution from a spinneret. The solution is ejected toward a grounded target and as the solution evaporates a nonwoven sheet of fibers is formed. Fiber diameter can be controlled by spinneret size and distance from the spinneret to the grounded collector as well as concentration, applied voltage, temperature, and humidity.[40] The thickness of the fiber mat can be controlled by spinning duration.

This paper describes the preparation of magnetic nonwoven fiber mat and filter paper by electrospinning. The as synthesized garnet nanoparticles were dispersed in cellulose acetate polymer solutions and electrospun on aluminum foil substrates resulting in free-standing nonwoven mats or on filter paper substrates to prepare magnetic filter paper. The electrospun composite fibers can be used in variety of biomedical applications such as magnetic cell and protein separations, and magnetic filters, and so forth. The magnetic filter paper was tested for the separation of fluorescein isothiocyanate (FITC) labeled bovine serum albumin (BSA) using an external magnet in an aqueous carbonate solution.

EXPERIMENTAL SECTION

Materials. Yttrium(III) nitrate hexahydrate, gadolinium(III) nitrate hexahydrate, sodium hydroxide, ethylene glycol, cellulose acetate (molecular weight 50000 g/mol), albumin from bovine serum, fluorescein isothiocyanate, sodium carbonate, sodium chloride, potassium phosphate monobasic, and potassium dihydrogen phosphate were purchased from the Aldrich Chemical Co. Iron(III) nitrate hexahydrate was purchased from Acros organics. Dimethylacetamide (DMAC) and acetone were purchased from Fisher Scientific. All reagents were used as received. Cellulose membranes (cutoff 10 kDa) were purchased from Fisher Scientific.

Synthesis of YIG and YGIG Nanoparticles. YIG nanoparticles were synthesized by modifying a reported procedure.[41] Stoichiometric mixtures (5:3) of 1 M nitrates of iron(III) (5 mL) and yttrium(III) (3 mL) were mixed with ethylene glycol (21 mL) at room temperature with stirring. Then 6 M NaOH (10 mL) were added dropwise to form the YIG precipitate. The product was centrifuged and washed with deionized water, then dried at 100 °C overnight. The YIG was annealed in air at 900 °C for 3 h. Stoichiometric mixtures (5:1.5:1.5) of 1 M nitrates of iron(III) (10 mL) and yttrium(III) (3 mL) and gadolinium(III) (3 mL) were used to synthesize YGIG nanoparticles based on the method described above.

Electrospinning of Polymer Solutions with YIG and YGIG Nanoparticles. YIG and YGIG nanoparticles were dispersed in a mixture of dimethylacetamide (DMAC) and acetone (2:3 v/v; total volume 10 mL) and 5, 10, and 20% weight/total volume dispersions were prepared by probe sonication at room temperature (Table 1).

Table 1. Composition of YIG/YGIG Nanoparticles Dispersed Polymer Solutions and Electrospinning Parameters

cellulose acetate (g)	garnet nanoparticles (g)	volume ratio DMAC: acetone	rate (mL/h)	voltage (kV)	electrode separation distance (cm)
1.4	0.5 YIG	2:3	0.05	14	6
1.3	1.0 YIG	2:3	0.05	14	6
1.2	2.0 YIG	2:3	0.05	14	6
1.4	1.0 YGIG	2:3	0.1	14	6
1.2	2.0 YGIG	2:3	0.1	14	6

The suspension of nanoparticles was placed in a scintillation vial and kept in an ice bath. The vial was covered using aluminum foil once the probe of the sonicator was placed inside the mixture to avoid volatilization of the solvent mixture. YIG nanoparticles were probe sonicated for 5 min to make a good dispersion of nanoparticles, and it was observed in normalized powder X-ray diffraction (PXRD) patterns that 12% crystallinity of initial YIG material had been lost due to the probe sonication (Supporting Information, Figure S1). YGIG nanoparticles were probe sonicated for 5 min to make a good dispersion of nanoparticles, and it was observed in normalized PXRD

patterns that 8% crystallinity of initial YGIG material had been lost due to the probe sonication (Supporting Information, Figure S2)

Cellulose acetate (CA) polymer was mixed manually with all the YIG and YGIG dispersions as shown in the Table 1.

The resulting polymer solutions were then loaded into a syringe with a 20 gauge needle. A voltage of 14 kV was applied to the spinneret. The fibers were collected on a rotating drum covered with Al foil and filter paper at 6 cm working distance to produce magnetic nonwoven fiber mats and magnetic filter papers.

Labeling of Bovine Serum Albumin (BSA) Using Fluorescein Isothiocyanate (FITC). BSA (100 mg) was labeled with FITC (2.5 mg) in 0.1 M carbonate buffer (50 mL) (pH 9) at room temperature and kept in the dark for 8 h at 4 °C. The FITC-BSA solutions were dialyzed with cellulose membranes using 1 L of phosphate buffered saline (PBS) at pH 7.4 (PBS was prepared using sodium chloride, potassium phosphate monobasic, and potassium dihydrogen phosphate) four times in 1 d in the dark at 4 °C to remove any unbound FITC. The light absorption at 495 nm was finally below 0.003 for the PBS solution. The concentration and F:P molar ratio were determined according to the methods described by the manufacturer using the albumin extinction coefficient 0.66 mg^{-1} mL^{-1} cm^{-1} at 279 nm.[42]

$$\frac{F}{P} = \frac{(MW/389)X(A_{495}/195)}{[(A_{280} - (0.35X A_{495}))/E^{0.1\%}]}$$

Where MW is the molecular weight of the protein, 389 is molecular weight of FITC, 195 is the absorption $E^{0.1\%}$ of bound FITC at 490 nm, $(0.35 \times A_{495})$ is the correction factor due to the absorbance of FITC at 280 nm (Supporting Information, Figure S12), $E^{0.1\%}$ is the absorption at 280 nm of a protein. Supporting Information, Table S1 and Figure S13 confirm the removal of unbound FITC. The calculated molar ratio of FITC:BSA is 0.3.

Testing the Magnetic Filter Paper with Electrospun Fibers As a Magnetic Carrier for FITC-BSA Separation. A 1 cm × 1 cm size piece of magnetic filter paper and magnetic fiber mat (10% YIG loaded) was soaked in FITC-BSA solution for 1 min and retrieved using a simple magnet stir bar retriever. A 1 cm^2 size of normal filter paper was used as a control. FITC-BSA bound filter paper was soaked in deionized water (10 mL) and retrieved using a simple magnet stir bar retriever. The isolated target compound was characterized.

Characterization. The X-ray diffraction patterns were collected on a Rigaku Ultima IV X-ray diffractometer using Cu Kα radiation. The morphology of the synthesized YIG, YGIG nanoparticles, and electrospun fibers were analyzed using scanning electron microscopy (SEM) and transmission electron microscopy (TEM). SEM analysis of Au/Pd coated samples were carried out using a Zeiss-LEO model 1530 SEM. TEM analysis was performed on JEOL 2100 analytical TEM with an accelerating voltage of 200 kV. The magnetic properties of the garnet nanoparticles and fibers were measured using a superconducting quantum interference device (SQUID) MPMS-XL from Quantum Design and the saturation magnetization (M_s), remnance (M_r), and coercivity (H_c) were determined from the hysteresis loops. Also magnetic susceptibility (χ_m), and relative permeability (μ_r) were calculated from the linear slope of $M(H)$ curve. Ultraviolet−visible spectrophotometry (UV/vis) was performed on Shimadzu UV-1601PC, and fluorescence was measured using Perkin-Elmer luminescence spectrometer LS50B with a 1 cm quartz cell.

RESULTS AND DISCUSSION

YIG and YGIG Nanoparticles. Figures 2 and 3 show the PXRD patterns for the as synthesized YIG and YGIG samples. The phases match well with $Fe_5Y_3O_{12}$ (JCPDS 00-033-0693) and $YGd_2Fe_5O_{12}$ (JCPDS 04-006-3735).

The crystallite sizes were calculated from the PXRD line broadening of the peak (420) using the Scherrer equation, $D_{hkl} = k\lambda/B\cos\theta$, where D_{hkl} is the particle size in nm, k is a constant (shape factor) with a value of 0.9, B is the width of half-maximum, and λ is the wavelength of the X-rays. The D_{hkl} values of YIG and YGIG are about 30 and 70 nm, respectively.

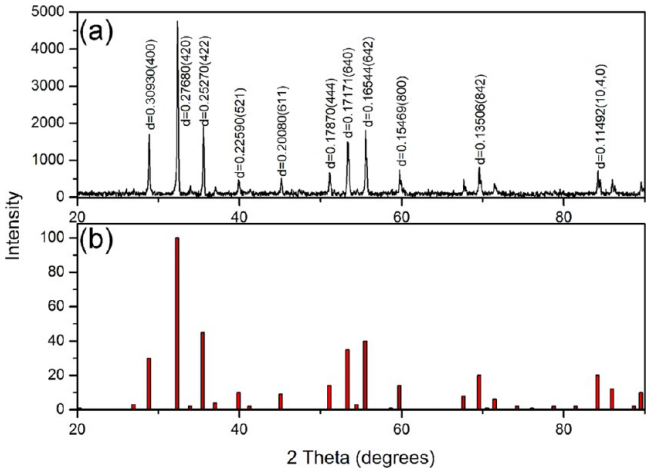

Figure 2. PXRD pattern of (a) YIG powder and (b) $Fe_5Y_3O_{12}$; JCPDS 00-033-0693.

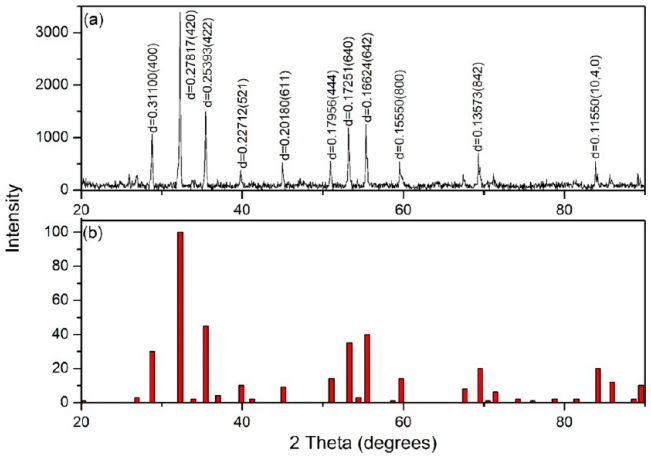

Figure 3. PXRD pattern of (a) YGIG powder and (b) $YGd_2Fe_5O_{12}$; JCPDS 04-006-3735.

TEM images of the as synthesized YIG and YGIG nanoparticles are shown in Figure 4. The nanoparticles generally exhibited a rounded irregular shaped morphology. The size distribution of YIG and YGIG are 30−40 nm and 60−70 nm respectively, which agrees with the values of 30 and 70 nm calculated from PXRD.

The interplanar distance of YIG is 0.28 nm (Figure 4 b) and YGIG is 0.27 nm (Figure 4 d) which corresponds to the (420) plane d = 0.2768 nm in Figure 2 and d = 0.2782 nm in Figure 3 respectively.

It has been reported that the size of the YIG particles synthesized using citrate gel containing ethylene glycol varied from 20−500 nm with the annealing temperature. The reported size of the YIG particles was between 100−500 nm when the annealing temperature was between 800−1000 °C.[41] Here the results indicate that nanocrystalline YIG and YGIG powders were successfully prepared by the hydroxide coprecipitation method. The synthesized YIG and YGIG were olive green and are magnetic as demonstrated by the attraction of the powder to a magnet as shown in Supporting Information, Figure S3.

The magnetization of the synthesized YIG and YGIG powders was performed at room temperature. Plots of magnetization (M) (normalized to the mass of magnetic material) as a function of magnetic field (H) are shown in

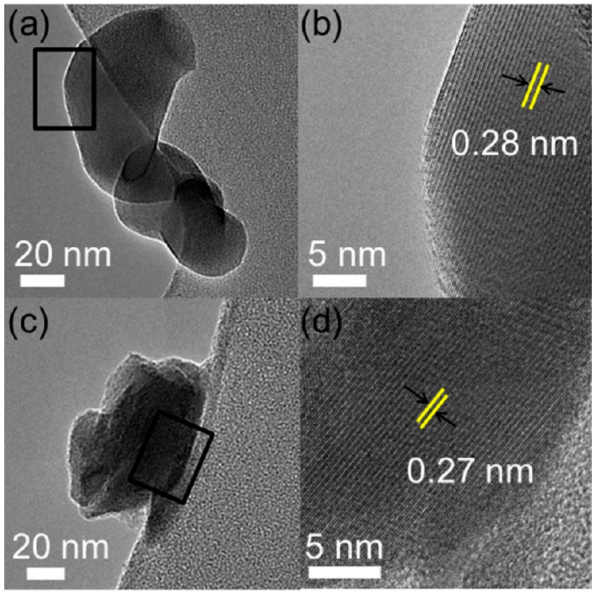

Figure 4. TEM images of as synthesized (a), (b) YIG; (c), (d) YGIG.

Figure 5. The saturation magnetization (M_s) is defined at the state when an increase in the magnetic field cannot increase the

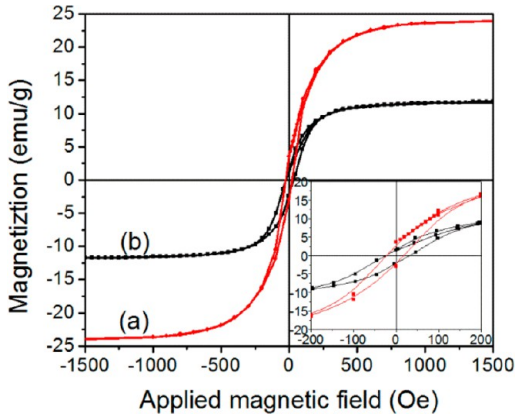

Figure 5. M−H hysteresis loops of the synthesized (a) YIG and (b) YGIG at room temperature.

magnetization of the material further. M_s reached 24.5 emu/g for YIG with the average particle size of 30 nm and 11.8 emu/g for YGIG with the average particle size of 70 nm. The coercive field (H_c, the external magnetic field required to bring the magnetization to zero) was 40 Oe for YIG and 58 Oe for YGIG. The reported saturation magnetization of YIG particles with an average 25 nm size was 20.6 emu/g and the coercivity is 51 Oe.[17] It is also reported that the saturation magnetization of the YIG samples, with particle sizes in the range 45−450 nm, decreases with decreasing particle size.[43]

In YGIG the saturation magnetization (M_s) decreases with the increase in the Gd concentration in a linear manner, and this can be related to the fact that the magnetic moments of Gd^{3+} ions align oppositely to the effective moments formed by Fe^{3+} ions.[16] The remnant magnetization (M_r) was 3.6 emu/g for YIG and 1.6 emu/g for YGIG. The calculated magnetic susceptibility (χ_m) using the linear part of the magnetization slope[44] was 4.23 and 2.88 and relative permeability ($\mu_r = 1 + \chi_m$) was 5.23 and 3.88 for YIG and YGIG, respectively. A relative permeability value of 5.3 has previously been reported for YIG prepared using a sol−gel technique.[45] At room temperature YIG nanoparticles show higher magnetic saturation, susceptibility, and relative permeability as compared to YGIG nanoparticles. These results are consistent with the room temperature soft ferromagnetic behavior of these materials.[17]

Electrospinning of CA Containing YIG Nanoparticles. Cellulose-based materials are widely used in the biopharmaceutical processing industry as the base matrix for adsorbent beads and membranes. Surface functionalized cellulose acetate nanofibers produced by electrospinning have been successfully used for bioseparations, where it was reported that CA nanofibers exhibit a high dynamic adsorption capacity.[46] SEM images of the electrospun fiber mats with different YIG nanoparticles loadings are shown in Figure 6 (a-1, b-1, c-1). As shown in the histogram 90% of fibers are below 150 nm. The average diameter of nanofibers are 75 ± 50 nm, 87 ± 40 nm, and 110 ± 44 nm when the YIG loadings in the liquid solution were 5%, 10%, and 20%. The increase in the fiber diameter with increasing YIG content may reflect the size of the 30 nm magnetic garnet nanoparticles as well as agglomeration. Agglomeration of nanoparticles was reported for electrospun poly(acrylonitrile-co-acrylic acid) fibers with palladium nanoparticles.[47]

The nanofibers prepared by electrospining have several advantages including high aspect ratio, high specific surface area, unique physiochemical properties, and design flexibility for chemical/physical surface functionalization.[48] Thus, the electrospun nanofibers are promising for bioseparations. The high surface area and high aspect ratio enhances the binding of biomolecules from biosuspensions. Also the fiber flexibility and chemical/physical surface functionalization are added advantages over currently available magnetic bioseparation methods.

The XRD patterns of the electrospun fibers with different loadings of YIG nanoparticles shown in Supporting Information, Figure S4 further confirm the presence of YIG nanoparticles in nanofibers.

SEM images of the electrospun fibers on filter paper with different YIG nanoparticle loadings are shown in Supporting Information, Figure S5 (a-1 and a-2). As shown in the histograms, 90% of fibers are below 150 nm. The average diameter of nanofibers are 99 ± 40 nm, and 110 ± 45 nm when the YIG loading are 10%, and 20%. The increase in fiber diameter with loading may also be due to the agglomeration of nanoparticles inside the fibers as the loading of nanoparticles increases.[47] This suggests the nature of substrate (paper vs aluminum foil) has little or no effect on the resulting fibers. The fibers associated with the filter paper are micrometers in diameter and not visible in these images. As explained previously the electrospun nanofiber filter paper is a promising candidate for bioseparations. The application of electrospun nanofiber membranes for several bioseparations has previously been reported.[48]

The SEM images of a cross section of the 10% YIG loaded electrospun CA fibers on filter paper is shown in Figure 7. The thickness of the electrospun fiber layer on filter paper is between 80 and 120 μm. This thickness can be varied by changing the electrospinning time and drum rotation speed, and so forth. It should also be noted that the electrospun CA fibers are well adhered to the fibers of filter paper and cannot be peeled from the paper.

Supporting Information, Figure S6 (a, b) shows digital images of the electrospun fiber mat on Al foil and on filter

dx.doi.org/10.1021/am404066g | ACS Appl. Mater. Interfaces 2014, 6, 244−251

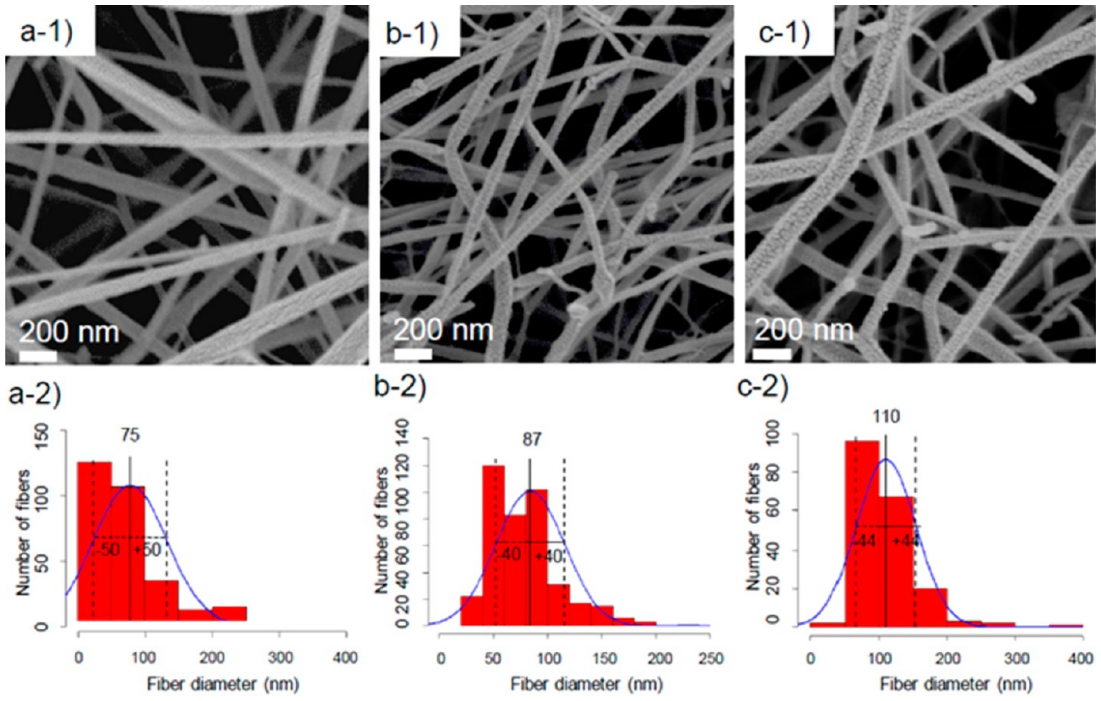

Figure 6. SEM images and fiber diameter distributions of (a-1, a-2) 5% YIG loaded, (b-1, b-2) 10% YIG loaded, (c-1, c-2) 20% YIG loaded electrospun fiber mats (using 20 images).

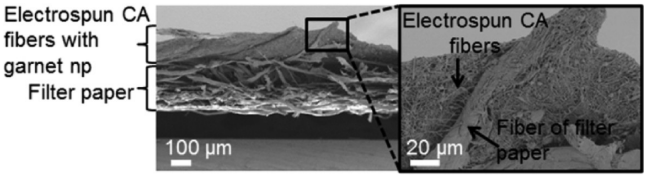

Figure 7. SEM image of a cross-section of the 10% YIG loaded electrospun fibers on filter paper.

paper with 10% YIG and YGIG loading, respectively. Supporting Information, Figure S6 (c, d) shows that a piece of electrospun fiber mat and filter paper with electrospun fibers can be picked up by a magnet. This is an important feature for retrieving the paper from liquid media. This property provides an added advantage for bioseparations using nanofibers since the bound compounds such as cells, proteins, and so forth on magnetic fibers can be easily and rapidly removed from biosuspensions using an appropriate magnetic separator. Compared with the other methods, the magnetic separation involves little mechanical stress and less time for separations.[49]

Supporting Information, Figure S7 shows the room temperature magnetic hysteresis loops of the freestanding YIG/CA nanofibers. Magnetization values have been normalized to the mass of magnetic material. The saturation magnetization (M_s) increases as the loading of YIG nanoparticles increases. The M_s values are 20.5, 22.4, and 24.5 emu/g for 10%, 20% YIG loaded electrospun CA fibers and YIG powder respectively (Supporting Information, Figure S7). The noticeably lower values in the saturation magnetization relative to the bulk powder could be ascribed to the isolated nature of embedded magnetic particles in the polymer matrix. It has been reported that saturate magnetization increases with increasing loading of magnetic nanoparticles, and there was a linear correlation between the saturate magnetization and loading of nanoparticles.[50] The extended separation between magnetic nanoparticles in a host polymer matrix reduces the dipolar coupling thereby preventing a cooperative ferromagnetic switching. The corresponding coercivity (H_c) values are 44, 46.5, and 40 Oe. This trend in coercivity was also observed for polyacrylonitrile fibers containing Fe_3O_4[51] and in carbon nanotubes decorated with magnetic nanoparticles. Apparently, part of the nanoparticles in CA fibers creates chains along the fibers with anisotropic dipolar interaction. This, so-called fanning mechanism, might be responsible for the coercivity enhancement in studied nanocomposites.[52] The remanence (M_r) values of 10% and 20% YIG/CA nanocomposite fibers are 1.60 and 2.27 emu/g. The calculated magnetic susceptibility values are 3.93 and 4.02 for 10% and 20% YIG/CA nanocomposite fibers, respectively. The corresponding calculated relative permeability values are 4.93 and 5.02. It was also reported that the relative permeability increased with increasing loading of nanoparticles on fibers.[50] The appearance of a hysteresis loop in the YIG powder and YIG/CA nanocomposite indicates that the averaged particle size of 30 nm is still above the superparamagnetism regime but close to the single domain regime with reduced M_s. Accordingly we can conclude that the magnetic properties of YIG garnet nanoparticles were successfully transferred into the electrospun nanofibrous mats.

Electrospinning of CA Containing YGIG Nanoparticles. SEM images of electrospun CA fibers on aluminum foil and filter paper containing 10% (w/v) YGIG nanoparticle loadings are shown in Supporting Information, Figure S8 (a-1 and a-2). As shown in the histogram (Supporting Information, Figure S8; b-1, and b-2), 80% of the fibers are below 150 nm. The average diameter of the nanofibers are 96 ± 42 nm for fiber deposited on aluminum foil and 114 ± 37 nm for fibers on filter paper when the YGIG loading is 10%. This is consistent with the large size of the YGIG nanoparticles (70 nm). PXRD (Supporting Information, Figure S9) also confirms the presence of YGIG nanoparticles in the fibers.

Supporting Information, Figure S10 shows the room temperature magnetic hysteresis loops of the YGIG/CA nano fibers. Magnetization values were normalized to the mass of magnetic material. The saturation magnetization (M_s) increases as the loading of YGIG nanoparticles increases. The M_s values are 5.4, 6.2, and 11.8 emu/g for 10%, and 20% YGIG loaded electrospun CA fibers and YGIG nanoparticles respectively (Supporting Information, Figure S10). YGIG/CA nanofibers have low saturate magnetization as compared to the YIG/CA nanofibers. This is due to the alignment of magnetic moment of Gd^{3+} ions oppositely to the effective moments formed by Fe^{3+} ions in YGIG nanoparticles. The corresponding coercivity (H_c) values are 65 and 70 Oe for 10% and 20% YGIG/CA nanocomposite fibers, respectively. This trend may be again due to some interaction with chains of nanoparticles. YGIG/CA nanofibers have higher coercivity as compared to YIG/CA fibers because of intrinsic structural anisotropy. The remnance (M_r) values of 10% and 20% YGIG/CA nanocomposite fibers are 2.8 and 3.0 emu/g. The calculated magnetic susceptibility values are 1.56 and 2.23 for 10% and 20% YGIG/CA nanocomposite fibers, respectively, and the corresponding calculated relative permeability values are 2.56 and 3.23. At room temperature, the YGIG/CA nanocomposites show low magnetic saturation, susceptibility, and relative permeability as compared to the YIG/CA nanocomposites but with higher coercivity. Thus the YIG/CA nanocomposites might be expected to be more effective magnetic nanocomposite materials for bioseparations because of higher magnetic properties compared with the YGIG/CA electrospun fibers at low applied field and at room temperature.

Testing the Magnetic Filter Paper with Electrospun Fibers As a Magnetic Carrier for FITC-BSA Separation. Figure 8 shows the magnetic electrospun nonwoven fiber mats, and filter paper can be retrieved using a simple magnet stir bar retriever.

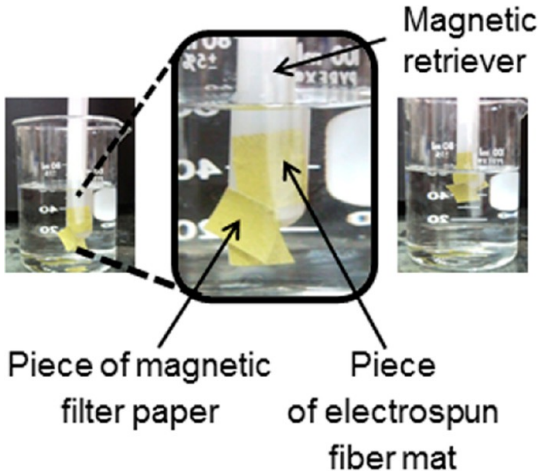

Figure 8. Digital images of pieces of magnetic filter paper dipped in NaCl salt solution adhering to a magnetic stir bar retriever.

The magnetic papers could be applied to liquid solutions, such as biological suspensions containing cells, proteins, and so forth, which need to be separated. Following a period when the target compound binds to the magnetic fibers, the whole magnetic complex is easily and rapidly removed from the sample using an appropriate magnetic separator. After washing out the contaminants, the isolated target compound can be eluted and used for further work. Magnetic nanoparticles embedded in polysaccharide-based hydrogels were reported for magnetically assisted bioseparations. Furthermore, bovine serum albumin was used as a model protein to illustrate the bioseparation.[8] Also covalent conjugated bovine serum albumin and magnetic nanoparticles in chitosan hydrogels were used for magnetically assisted bioseparations.[53] The magnetic hydrogel is easily swollen in the biosuspensions and may become difficult to handle and use for longer times. In contrast, the electrospun magnetic fibers do not have such problems, and they are easily handled.

To demonstrate this, 1 cm × 1 cm size pieces of magnetic filter paper and magnetic fiber mat were used as magnetic carriers to separate FITC-BSA from carbonate solutions (Supporting Information, Figure S11). One cm^2 size of plain filter paper was used as a control. Bovine serum albumin (BSA) is a globular protein (~66,000 Da) that is used in numerous biochemical applications because of its stability and lack of interference with biological reactions. Fluorescein isothiocyanate (FITC) is widely used as a fluorescent label for proteins.[54] FITC labeled BSA was previously used to demonstrate bioseparations using silica coated magnetic nanoparticles.[55]

Figure 9 (a) shows a digital image of fluorescent FITC-BSA bound filter paper under a black light (254 nm). The FITC-

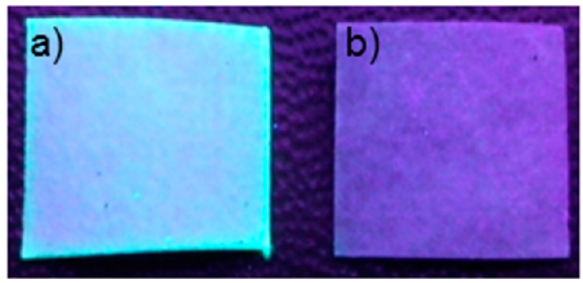

Figure 9. Digital images of (a) FITC-BSA bound filter paper and (b) filter paper after dipping in deionized water under UV irradiation at 254 nm.

BSA magnetic filter paper can then be washed to recollect the FITC-BSA.

Figure 9 (b) shows the washed magnetic paper which is no longer fluorescent. This confirms that FITC-BSA that was bound to the magnetic filter paper was washed out successfully. UV/vis spectroscopy was carried out (Supporting Information, Figure S12b) to determine the amount of bound protein to the magnetic filter paper. It was found that 0.0069, 0.0054, and 0.0039 μmol of BSA can be separated by 1 cm^2 size piece of filter paper coated with magnetic electrospun fibers, a magnetic electrospun fiber mat, and a control of plain filter paper. Magnetic filter paper with electrospun CA fibers and magnetic electrospun CA fiber mat absorb higher percentages of BSA compared to the plain filter paper. This is due to the interaction of BSA with the higher surface area nanofibers as compared to the micrometer size fibers in normal filter paper. CA is a popular substrate for adsorptive membranes with hydrophilic surfaces. It has been reported that there is a higher affinity of proteins for hydrophobic surfaces than hydrophilic surfaces such as for adsorption of BSA onto polystyrene latex and hematite, human serum albumin onto silicon wafers, BSA onto silica gel, human fibrinogen onto polyethylene foil and glass plate, BSA onto glass plate, and BSA onto hydrophobic calcium hydroxyapatites.[56] It has also been noted that adsorption of

protein on polymer surfaces may be affected by hydrophobic interactions as well as electrostatic repulsion.[57] It has been reported that the hydrophobic interaction between BSA and cellulose acetate butyrate (CAB) might overcome the electrostatic repulsion, leading to a higher amount of absorption of BSA on CAB.[58] Therefore, the hydrophobic adsorption of FITC labeled BSA on CA magnetic fibers is possible, which can be used to separate FITC-BSA from carbonate solution. Furthermore, there is no strong chemical bonding between FITC-BSA and CA fibers. Thus, the FITC-BSA can be easily removed from the mat by simply dipping the mat in deionized water several times. The filter paper coated with magnetic electrospun CA fibers and freestanding magnetic electrospun CA fiber mats were stable even after several (10 trials) FITC-BSA separations. This further confirms the good interaction between the electrospun CA fibers and the filter paper as explained in Figure 7.

The FITC-BSA bound filter paper soaked in deionized water were analyzed using TEM to check whether there is any loss of the embedded nanoparticles from the CA fibers. There were no free nanoparticles detected in the samples. Also no accumulation of particles in the above sample solutions was detected in the presence of an external magnetic field. This confirms that there was no leakage of the embedded nanoparticles from the CA fibers when soaked in the biological solutions.

A distinct advantage of magnetic separation is that the sample is subjected to very little mechanical stress as compared to with the other methods. Flexible magnetic nanohybrid membranes with an amphiphobic surface based on bacterial cellulose and Fe_3O_4 nanoparticles[13] and magnetically assisted hydrogels[8] have also been reported for bioseparation. The surface of magnetic cellulose acetate nanofibers and filter paper can be easily functionalized for bioseparations because of the high surface area to volume ratio and the rich surface chemistry of cellulose acetate nanofibers.

CONCLUSIONS

Novel magnetic nonwoven fiber mats and filter paper were successfully prepared for the first time by electrospinning biocompatible cellulose acetate polymer solutions with YIG and YGIG nanoparticles. By changing the amount of YIG and YGIG nanoparticles the size and magnetic properties of electrospun magnetic nanofibers could be varied. The resultant magnetic nanopolymer composite fibers can be used for magnetically assisted bioseparations such as for BSA as shown above.

ASSOCIATED CONTENT

Supporting Information

PXRD pattern of electrospun fibers with 20%, 10%, 5% YIG and 20%, 10% YGIG; normalized PXRD patterns of probe sonicated YIG and YGIG powders; digital image of YIG and YGIG powder attracted to a magnet; SEM images and fiber diameter distributions of 10% YIG and 20% YIG loaded electrospun fiber on filter paper; SEM images and fiber diameter distributions of 10% YGIG loaded electrospun CA fiber mat and 10% YGIG loaded electrospun fiber on filter paper; digital image of 10% YIG electrospun fiber mat on Al foil, filter paper with 10% YIG electrospun fibers, a piece of electrospun fibers mat and a piece of filter paper with electrospun fibers picked up by a magnet; M−H hysteresis loops of the YIG powder, freestanding electrospun fibers with 20% YIG, electrospun fibers with 10% YIG, YGIG powder, electrospun fibers with 20% YGIG, and electrospun fibers with 10% YGIG; UV/vis and fluorescence spectra of FTIC, FITC-BSA, BSA; digital images of picking up of pieces of magnetic filter paper dipped in FITC-BSA solution under black light. This material is available free of charge via the Internet at http://pubs.acs.org.

AUTHOR INFORMATION

Corresponding Author

*E-mail: balkus@utdallas.edu.

Notes

The authors declare no competing financial interest.

ACKNOWLEDGMENTS

This work was financial supported by the Robert A.Welch Foundation-AT1153.

REFERENCES

(1) Honda, H.; Kawabe, A.; Shinkai, M.; Kobayashi, T. *J. Ferment. Bioeng.* **1998**, *86*, 191−196.
(2) Bucak, S.; Jones, D. A.; Laibinis, P. E.; Hatton, T. A. *Biotechnol. Prog.* **2003**, *19*, 477−484.
(3) Lutz, J. F.; Stiller, S.; Hoth, A.; Kaufner, L.; Pison, U.; Cartier, R. *Biomacromolecules* **2006**, *7*, 3132−3138.
(4) Pinchuk, L. S.; Markova, L. V.; Gromyko, Y. V.; Markov, E. M.; Choi, U. S. *J. Mater. Process. Technol.* **1995**, *55*, 345−350.
(5) Epstein, A. J.; Miller, J. S. *Synth. Met.* **1996**, *80*, 231−237.
(6) Sonehara, M.; Noguchi, S.; Kurashina, T.; Sato, T.; Yamasawa, K.; Miura, Y. *IEEE Trans. Magn.* **2009**, *45*, 4173−4175.
(7) Saiyed, Z. M.; Telang, S. D.; Ramchand, C. N. *Biomagn. Res. Technol.* **2003**, *1*, 2.
(8) Liang, Y. Y.; Zhang, L. M.; Jiang, W.; Li, W. *ChemPhysChem* **2007**, *8*, 2367−2372.
(9) Bao, F.; Yao, J.-L.; Gu, R.-A. *Langmuir* **2009**, *25*, 10782−10787.
(10) Son, S. J.; Reichel, J.; He, B.; Schuchman, M.; Lee, S. B. *J. Am. Chem. Soc.* **2005**, *127*, 7316−7317.
(11) Yang, H.-H.; Zhang, S.-Q.; Chen, X.-L.; Zhuang, Z.-X.; Xu, J.-G.; Wang, X.-R. *Anal. Chem.* **2004**, *76*, 1316−1321.
(12) Bruce, I. J.; Sen, T. *Langmuir* **2005**, *21*, 7029−7035.
(13) Zhang, W.; Chen, S.; Hu, W.; Zhou, B.; Yang, Z.; Yin, N.; Wang, H. *Carbohydr. Polym.* **2011**, *86*, 1760−1767.
(14) Komori, T.; Sakakura, T.; Takenaka, Y.; Tanaka, K.; Okuda, T. *Acta Crystallogr., Sect. E* **2009**, *65*, 72.
(15) Lee, Y. B.; Chae, K. P.; Lee, S. H. *J. Phys. Chem. Solids.* **2001**, *62*, 1335−1340.
(16) Cheng, Z.; Yang, H.; Yu, L.; Cui, Y.; Feng, S. *J. Magn. Magn. Mater.* **2006**, *302*, 259−262.
(17) Rajendran, M.; Deka, S.; Joy, P. A.; Bhattacharya, A. K. *J. Magn. Magn. Mater.* **2006**, *301*, 212−219.
(18) Wu, Y. J.; Fu, H. P.; Hong, R. Y.; Zheng, Y.; Wei, D. G. *J. Alloys Compd.* **2009**, *470*, 497−501.
(19) Pal, M.; Chakravorty, D. *Phys. E (Amsterdam, Neth.)* **1999**, *5*, 200−203.
(20) Vaqueiro, P.; Lopez-Quintela, M. A. *J. Mater. Chem.* **1998**, *8*, 161−163.
(21) Vaqueiro, P.; Lopez-Quintela, M. A.; Rivas, J. *J. Mater. Chem.* **1997**, *7*, 501−504.
(22) Wang, S.; Xu, Y.; Lu, P.; Xu, C.; Cao, W. *Mater. Sci. Eng., B* **2006**, *127*, 203−206.
(23) Guo, X. Z.; Ravi, B. G.; Devi, P. S.; Hanson, J. C.; Margolies, J.; Gambino, R. J.; Parise, J. B.; Sampath, S. *J. Magn. Magn. Mater.* **2005**, *295*, 145−154.
(24) Amighian, J.; Hasanpour, A.; Mozaffari, M. *Phys. Status Solidi C* **2004**, *1*, 1769−1771.
(25) Rashad, M. M.; Hessien, M. M.; El-Midany, A.; Ibrahim, I. A. *J. Magn. Magn. Mater.* **2009**, *321*, 3752−3757.

(26) Chen, M.; Qu, H.; Zhu, J.; Luo, Z.; Khasanov, A.; Kucknoor, A. S.; Haldolaarachchige, N.; Young, D. P.; Wei, S.; Guo, Z. *Polymer* **2012**, *53*, 4501−4511.
(27) Chhabra, R.; Isele, O. E. A. *Coated Nanofiber Webs*. U.S. Patent 20050008776A1, Jan 13, 2005.
(28) Pisignano, D.; Maruccio, G.; Mele, E.; Persano, L.; Di Benedetto, F.; Cingolani, R. *Appl. Phys. Lett.* **2005**, *87*, 1−3.
(29) Feng, L.; Li, S.; Li, H.; Zhai, J.; Song, Y.; Jiang, L.; Zhu, D. *Angew. Chem., Int. Ed.* **2002**, *41*, 1221−1223.
(30) Martin, C. R. *Chem. Mater.* **1996**, *8*, 1739−1746.
(31) Faul, C. F. J.; Antonietti, M. *Adv. Mater.* **2003**, *15*, 673−683.
(32) Huang, J.; Kaner, R. *J. Am. Chem. Soc.* **2003**, *126*, 851−855.
(33) Anka, F. H.; Perera, S. D.; Ratanatawanate, C.; Balkus, K. J., Jr. *Mater. Lett.* **2012**, *75*, 12−15.
(34) Tran, D.; Balkus, K. J., Jr. *Top. Catal.* **2012**, *55*, 1057−1069.
(35) Shariatpanahi, S. P.; Iraji zad, A.; Abdollahzadeh, I.; Shirsavar, R.; Bonn, D.; Ejtehadi, R. *Soft Matter* **2011**, *7*, 10548−10551.
(36) Liu, H. A.; Balkus, K. J., Jr. *Mater. Lett.* **2009**, *63*, 2361−2364.
(37) Sill, T. J.; von Recum, H. A. *Biomaterials* **2008**, *29*, 1989−2006.
(38) Agarwal, S.; Wendorff, J. H.; Greiner, A. *Polymer* **2008**, *49*, 5603−5621.
(39) Lee, K. Y.; Jeong, L.; Kang, Y. O.; Lee, S. J.; Park, W. H. *Adv. Drug Delivery Rev.* **2009**, *61*, 1020−1032.
(40) Lu, P.; Ding, B. *Recent Pat. Nanotechnol.* **2008**, *2*, 169−182.
(41) Vaqueiro, P.; Crosnier-Lopez, M. P.; Lopez-Quintela, M. A. *J. Solid State Chem.* **1996**, *126*, 161−168.
(42) Hungerford, G.; Benesch, J.; Mano, J. F.; Reis, R. L. *Photochem. Photobiol. Sci.* **2007**, *6*, 152−158.
(43) Sanchez, R. D.; Rivas, J.; Vaqueiro, P.; Lopez-Quintela, M. A.; Caeiro, D. *J. Magn. Magn. Mater.* **2002**, *247*, 92−98.
(44) Nguyet, D. T. T.; Duong, N. P.; Satoh, T.; Anh, L. N.; Hien, T. D. *J. Magn. Magn. Mater.* **2013**, *332*, 180−185.
(45) Yahya, N.; Al Habashi, R. M.; Koziol, K.; Borkowski, R. D.; Akhtar, M. N.; Kashif, M.; Hashim, M. *J. Nanosci. Nanotechnol.* **2011**, *11*, 2652−2656.
(46) Zhang, L.; Menkhaus, T. J.; Fong, H. *J. Membr. Sci.* **2008**, *319*, 176−184.
(47) Demir, M. M.; Gulgun, M. A.; Menceloglu, Y. Z.; Erman, B.; Abramchuk, S. S.; Makhaeva, E. E.; Khokhlov, A. R.; Matveeva, V. G.; Sulman, M. G. *Macromolecules* **2004**, *37*, 1787−1792.
(48) Menkhaus, T. J.; Zhang, L.; Fong, H. *Applications of Electrospun Nanofiber Membranes for Bioseparations*; Nova Science Pub Inc: New York, 2010; pp 1−36.
(49) Saiyed, Z. M.; Ramchand, C. N.; Telang, S. D. *J. Phys.: Condens. Matter* **2008**, *20*, 1−5.
(50) Gupta, P.; Asmatulu, R.; Claus, R.; Wilkes, G. *J. Appl. Polym. Sci.* **2006**, *100*, 4935−4942.
(51) Zhang, D.; Karki, A. B.; Rutman, D.; Young, D. P.; Wang, A.; Cocke, D.; Ho, T. H.; Guo, Z. *Polymer* **2009**, *50*, 4189−4198.
(52) Klabunde, K. J. *Nanoscale Materials in Chemistry*; John Wiley & Sons: New York, 2001; pp 200−204.
(53) Ghaemy, M.; Naseri, M. *Carbohydr. Polym.* **2012**, *90*, 1265−1272.
(54) Wang, C.; Ouyang, J.; Ye, D. K.; Xu, J. J.; Chen, H. Y.; Xia, X. H. *Lab Chip* **2012**, *12*, 2664−2671.
(55) Lee, S. Y.; Ahn, C. Y.; Lee, J.; Lee, J. H.; Chang, J. H. *Nanoscale Res. Lett.* **2012**, *7*, 279.
(56) Kandori, K.; Mukai, M.; Fujiwara, A.; Yasukawa, A.; Ishikawa, T. *J. Colloid Interface Sci.* **1999**, *212*, 600−603.
(57) Kim, J. T.; Weber, N.; Shin, G. H.; Huang, Q.; Liu, S. X. *J. Food Sci.* **2007**, *72*, 214−221.
(58) Hashino, M.; Hirami, K.; Katagiri, T.; Kubota, N.; Ohmukai, Y.; Ishigami, T.; Maruyama, T.; Matsuyama, H. *J. Membr. Sci.* **2011**, *379*, 233−238.